

Robotic Slicing of Fruits and Vegetables: Modeling the Effects of Fracture Toughness and Knife Geometry

Prajjwal Jamdagni and Yan-Bin Jia

Abstract—Slicing is an important skill for a robot to learn as it is more efficient and results in less deformation in comparison with cutting by pressing. Cutting experiments with foods have indicated that the ease of slicing is caused by a decrease in fracture toughness. In this paper, we formally characterize this decrease based on the work needed to maintain the critical strain for fracture. Forces generating fracture and deformation and overcoming friction are predicted using FEM and based on fracture mechanics. Extending our previous work [1] on cutting by pressing with a straight knife edge, we model general slicing actions and knife geometry (i.e., a curved edge). Experiments over potatoes and eggplants have demonstrated the accuracy of modeling in predicting the overall cutting force during slicing, which could be leveraged for control of cutting by the robot to demonstrate human-level skills in the near future.

I. INTRODUCTION

In the food industry, there exists a great demand for workers who can prepare fruits and vegetables for cooking purpose. This is a tedious job with repetitive actions and long working hours, and thus has a large workforce turnover. In addition, the COVID-19 pandemic is placing an increasing focus on health, hygiene, and safety during food preparation. All these problems can be addressed by employing robots which can work tirelessly at this job in a safe and hygienic manner. Skills such as chopping and slicing will be essential for robots to work in this industry.

From our own experience, we know that slicing an object with a kitchen knife is a lot easier than pressing with it. Robots need to take advantage of the efficiency of the slicing action. In our previous work [1], a model was presented for cutting by (vertically downward) pressing with a straight knife edge based on fracture mechanics and the finite element method (FEM). The object was divided into several cross sections so cutting could be modeled as crack propagation independently within these 2-dimensional (2D) slices. This work, however, did not model more skillful moves such as slicing or the effect of knife geometry.

Atkins *et al.* [2] presented an energy-based analytical model of slicing. The authors made two assumptions. First, the cutting force and the knife displacement were coincident

*Support for this research has been provided by the US National Science Foundation under Grant IIS-1651792. Any opinions, findings, and conclusions or recommendations expressed in this material are those of the authors and do not necessarily reflect the views of the National Science Foundation.

*We would like to thank Xiaoqian Mu and Yuechuan Xue for their early help with the experiments. We also thank anonymous reviewers for their valuable feedback.

The authors are affiliated with the Department of Computer Science, Iowa State University, Ames, IA 50011, USA. prajjwal, jia@iastate.edu.

in the plane of cutting. This assumption does not appear to be true for cutting of deformable objects. The reason behind is that there exist different sources of origin for tangential and normal forces. While the normal force results from a normal compression, the tangential force results from shearing due to the friction between the knife edge and the object. We adopt generalized plane strain assumption to decouple the two forces [3], [4] and use FEM for calculation. The second assumption by Atkins *et al.* was that the fracture toughness of an object during slicing would always be the same as during pressing. Again, this is not true, as we have found in our experiments that the fracture toughness changes during slicing. Less deformation is required during slicing to reach the critical maximum principal strain for fracture [5], which in turn results in a decrease in the fracture toughness. In this paper, we characterize such decrease during slicing by examining the strain below the knife edge.

Our previous work [1] used a fixed set of cross sections, an approach no longer suitable for cutting with a curved knife edge. This is because a set of cross sections normal to the knife edge at one time instant will no longer be normal at the next instant as the edge slices through the object. In this paper, we tackle this issue by continuously updating the cross sections based on the current crack front and knife trajectory.

This paper focuses on modeling of slicing by a curved knife attached to a robotic arm. Section II discusses related works from fracture mechanics and soft tissue cutting. In Section III, the change in fracture toughness during slicing with a straight knife edge is characterized based on the maximum principal strain below the knife edge. In Section IV, slicing with a curved knife edge is modeled. Experimental results are presented in Section V. Section VI ends the paper with some directions for future research.

A vector is represented by a lowercase letter in bold, e.g., $\mathbf{p} = (p_x, p_y)^T$, with its x - and y -coordinates denoted by the same (non-bold) letter with subscripts x and y , respectively.

II. RELATED WORK

Soft tissue cutting is traditionally modeled as crack propagation based on fracture mechanics. Estimation of fracture toughness was done for ductile materials [6], and during the insertion of a needle into soft issue aided by FEM-based simulation [7]–[9]. FEM methods, both linear [10] and nonlinear [11], were used in surgical simulation of soft tissue cutting, with a comprehensive survey conducted in [12].

A model for compression cutting of bio-materials, and the effect of blade sharpness were presented [13]. Stress distribution and its effect on the fracture force during slicing

were also investigated [14], [15]. An energy-based model was employed to explain the reduction in fracture force due to slicing under the assumption of constant fracture toughness [2]. This model was used to predict the force and torque generated from slicing thin flexible materials with negligible deformations [16]. In paper industry, fracture mechanics is used to model crack propagation during the slicing of a paper stack and the effect of friction on facilitating the process [17], [18]. Reduction in frictional force during soft material cutting was found to be related to a large inclination angle of the blade [19].

Ease of slicing was attributed to the change from a global deformation during compression to a local shear deformation [5]. For soft tissues, slicing made it easier to achieve the critical stress or strain for fracture [20]. The aforementioned works all pointed at varying fracture toughness with slicing angle.

Investigations were conducted on strategies for robotic cutting based on adaptive control using position and velocity history [21] and impedance control for force tracking [22]. Soft material cutting has employed force/vision based control strategies for trajectory following and object stabilization [23], [24]. In [25] a three-phase cutting strategy was introduced to combine position, force, and impedance controls.

III. SLICING WITH A STRAIGHT KNIFE EDGE

In [1], we modeled the cutting of a deformable object when the knife edge is straight, horizontal (parallel to the z -axis as shown in Fig. 1), and translating downward in the vertical yz -plane, which coincides with the blade's plane of symmetry. Assuming plane strain at the contact between the knife edge and the object, we divided the object by multiple cross sections parallel to the xy -plane. Cutting of each cross section was modeled using linear elastic fracture mechanics:

$$dW = R_c ds + dU, \quad (1)$$

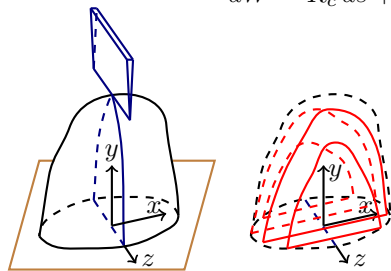


Fig. 1: Object represented by evenly spaced cross sections parallel to the xy -plane.

where dW is the work done by the knife for an infinitesimal movement dy , R_c is the fracture toughness, defined as the energy required to increase the crack by unit area, ds is the increment in crack length, and dU is the change in strain energy. It should be noted that since we are cutting a 2D cross section, force has the unit of N/m, and work and energy have the unit of N. We introduced an *energy release rate*, $R = (dW - dU)/ds$, to predict when the crack would propagate ($R > R_c$), and, if so, the extra crack length ds . FEM was used to calculate the strain energy and the force over a given mesh of the cross section. We integrated over all the cross sections to predict the total force by the knife edge. This work is referred to as “cutting by *pressing*”, where the knife velocity is normal to the knife edge.

where dW is the work done by the knife for an infinitesimal movement dy , R_c is the fracture toughness, defined as the energy required to increase the crack by unit area, ds is the increment in crack length, and dU is the change in strain energy.

In contrast, “cutting by *slicing*” refers to cutting when the knife’s velocity also has a component along its (straight) edge, that is, in the z -direction. This makes it easier to reach critical stress or strain for fracture at the contact [5]. The critical maximum principal strain has been found to maintain a relatively constant value for different ratios between normal and tangential force [20], [26]. Hence this strain is used to characterize the change in fracture toughness during slicing. The plane strain assumption used in our previous work [1] is replaced with the following generalized version to take tangential force into account:

(A1) All planes normal to the knife edge undergo the same deformation.

We also make a second assumption:

(A2) Deformation in the knife cutting plane, the yz -plane, only happens in the knife velocity direction.

We will only consider translations of the knife in this paper.

A. Strain Below the Knife Edge

To obtain the strain at a point p right below the knife edge within a cross section, we model the object as a half-space and the knife as a line slicing through the half-space. The contact between the knife edge and the object is a narrow infinite strip along the knife edge, as shown in Fig. 2. A local coordinate frame $x'y'z'$ is defined, such that the knife edge stretches along the x' -axis, and the z' -axis passes through the point p at which we want to characterize the strain. The angles θ_1 and θ_2 are between the z' -axis and the lines joining p with the endpoints of the segment intersected by the edge strip with the $y'z'$ -plane. Let σ_{ii} be the normal stress, where i is the direction of the normal stress, and σ_{ij} be the shear stress, where i is the direction of the normal to the plane in which the shear stress is applied and j is the direction of the shear stress. We also define two directions, \hat{n} , normal to the knife edge and coincident with the z' -axis, and \hat{t} , tangential to the knife edge and coincident with x' -axis. Let f_n and f_t be the normal and tangential forces per unit surface area, respectively, applied by the knife edge on the object.

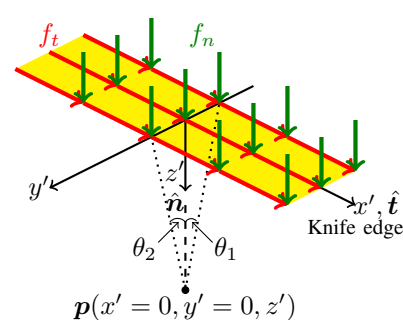


Fig. 2: Stress at a point due to normal and tangential strip loading.

Boussinesq [27] solved the problem of the stress at any point in an infinite half-space due to a normal point load on its boundary plane. This solution was integrated over the contact area between the knife edge and the object in [28] to calculate the stress due

to a normal strip loading f_n at p :

$$\begin{aligned}\sigma_{z'z'} &= (\theta_2 - \theta_1 + (\sin(2\theta_2) - \sin(2\theta_1))/2) f_n/\pi, \\ \sigma_{y'y'} &= (\theta_2 - \theta_1 - (\sin(2\theta_2) - \sin(2\theta_1))/2) f_n/\pi, \\ \sigma_{x'x'} &= \nu(\sigma_{y'y'} + \sigma_{z'z'}), \\ \sigma_{y'z'} &= \sigma_{z'y'} = (\sin^2 \theta_2 - \sin^2 \theta_1) f_n/\pi, \\ \sigma_{x'y'} &= \sigma_{y'x'} = \sigma_{z'x'} = \sigma_{x'z'} = 0,\end{aligned}\quad (2)$$

where ν is the Poisson's ratio.

Cerruti's solution for the stress at any point in an infinite half-space due to a tangential point load f_t at the surface is derived in [28]. We integrate this solution over the contact area between the knife edge and the object to obtain stress at p due to a tangential strip load:

$$\begin{aligned}\sigma_{x'z'} &= \sigma_{z'x'} = (\theta_2 - \theta_1) f_t/\pi, \\ \sigma_{x'y'} &= \sigma_{y'x'} = (\ln |\cos \theta_1| - \ln |\cos \theta_2|) f_t/\pi, \\ \sigma_{x'x'} &= \sigma_{y'y'} = \sigma_{y'z'} = \sigma_{z'z'} = 0.\end{aligned}\quad (3)$$

For a point just below the knife edge, $\theta_1 = -\pi/2$ and $\theta_2 = \pi/2$. Substituting these values into (2) and (3), we obtain

$$\begin{aligned}\sigma_{x'x'} &= 2\nu f_n, & \sigma_{y'y'} &= f_n, & \sigma_{z'z'} &= f_n, \\ \sigma_{x'y'} &= 0, & \sigma_{y'z'} &= 0, & \sigma_{z'x'} &= f_t.\end{aligned}$$

Using Hooke's law, the strain tensor can be calculated as

$$\epsilon = \frac{1}{E} \begin{pmatrix} 0 & 0 & f_t(1+\nu) \\ 0 & f_n(1-\nu-2\nu^2) & 0 \\ f_t(1+\nu) & 0 & f_n(1-\nu-2\nu^2) \end{pmatrix},$$

where E is the Young's modulus. The largest eigenvalue of this strain tensor gives us the maximum principal strain:

$$\begin{aligned}\epsilon_{\max} &= (f_n/2E) \left((1-\nu-2\nu^2) \right. \\ &\quad \left. + \sqrt{(1-\nu-2\nu^2)^2 + 4((f_t/f_n)(1+\nu))^2} \right).\end{aligned}\quad (4)$$

Instead of stress or strain, we use fracture toughness as a criterion for fracture because it approximates the plastic deformation at the crack front, and is easier to measure through experiment. Next, we will characterize the change in fracture toughness during slicing.

B. Varying Fracture Toughness With the Slice-Push Ratio

Atkins *et al.* [2] introduced the slice-push ratio ξ as the ratio between the knife's tangential displacement dt and normal displacement dn . They also assumed that it is equal to the ratio between the knife's tangential force F_t and normal force F_n , that is, $\xi = dt/dn = F_t/F_n$. But this is not the case for deformable objects. The tangential force is a shear force, and therefore proportional to the shear modulus G and the tangential displacement. On the other hand, the normal force is a compression force, and proportional to the Young's modulus E and the normal displacement. We propose the following new form of their ratio:

$$\frac{F_t}{F_n} = \frac{f_t}{f_n} = \frac{G}{E} \frac{dt}{dn} = \frac{1}{2(1+\nu)} \xi.$$

Substituting the ratio into (4), we get

$$\epsilon_{\max} = \frac{f_n}{2E} \left((1-\nu-2\nu^2) + \sqrt{(1-\nu-2\nu^2)^2 + \xi^2} \right).\quad (5)$$

The maximum principal strain for pressing ($\xi = 0$) and slicing ($\xi \neq 0$) can be derived from (5) respectively below:

$$\begin{aligned}\epsilon_{\max}^p &= \frac{f_n^p}{E} (1-\nu-2\nu^2), \\ \epsilon_{\max}^s &= \frac{f_n^s}{2E} \left((1-\nu-2\nu^2) + \sqrt{(1-\nu-2\nu^2)^2 + \xi^2} \right).\end{aligned}$$

As the critical maximum principal strain for fracture onset remains fixed [20], [26], we calculate the ratio between the normal forces during slicing and pressing for the same maximum principal strain as

$$f_n^s/f_n^p = 2/(1 + \sqrt{1 + (\xi/(1-\nu-2\nu^2))^2}).$$

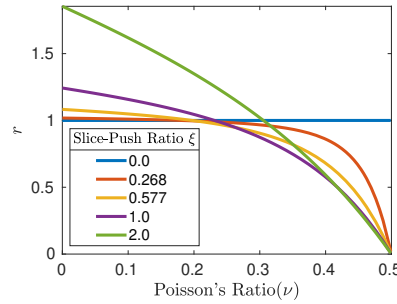


Fig. 3: Changing fracture toughness during slicing as measured by its ratio to the constant value during pressing.

During the continuous cutting of an infinite half-space, the change in strain energy is negligible and all the work done by the knife gets converted into extending the crack. As the state of critical maximum principal strain is constantly maintained at the knife edge, for the same vertical displacement dn , the ratio between the fracture toughness R_c^s for slicing and the fracture toughness R_c for pressing can be derived as

$$\begin{aligned}r &= \frac{R_c^s}{R_c} = \frac{(f_n^s dn + f_t^s dt)/dn}{(f_n^p dn)/dn} = \frac{f_n^s}{f_n^p} \left(1 + \frac{\xi^2}{2(1+\nu)} \right) \\ &= \frac{2}{1 + \sqrt{1 + (\xi/(1-\nu-2\nu^2))^2}} \left(1 + \frac{\xi^2}{2(1+\nu)} \right).\end{aligned}\quad (6)$$

Fig. 3 plots the value of r relative to Poisson's ratio for different ξ values.

C. Slicing a Cross section

The total work dW during slicing has a vertical component $dW_n = F_n dn$ and a horizontal component $dW_t = F_t dt$. We use the generalized plane strain condition [4] to decouple the two forces F_n and F_t . Just like F_n and dW_n were calculated using FEM in our previous work [1], F_t and dW_t can also be determined using FEM here as the antiplane shear component of generalized plane strain [4] by solving the Laplace equation, $\nabla^2 u_t = 0$, where u_t is the displacement in the tangential direction. Two boundary conditions are imposed. First, the bottom of the cross section is fixed. Second, the nodes in contact with the knife edge are fixed on it. For slicing, R will then be calculated as $R = (dW_n + dW_t - dU)/ds$. FEM is also used for calculating

dU . Also, the condition for crack propagation uses new fracture toughness R_c^s derived in (6). The crack propagates when $R > R_c^s = r R_c$.

The slicing of a cross section is modeled iteratively, similar to [1]. Within one iteration, the knife will move downward until the energy release rate R for a crack of very small depth δ exceeds the fracture toughness R_c^s . To determine the actual length of the crack, we increase δ in integer multiples until we find an interval that bounds the maximum crack length and then use bisection method to calculate ds such that $R = R_c^s$. This is repeated for each cross section and integrated over all cross sections to get total force as in [1].

IV. SLICING WITH A CURVED KNIFE EDGE

Until now, we have modeled slicing with a translating straight knife edge. A cross section normal to the edge will be normal to all the elements of the edge that it will come in contact with during slicing. Along a curved knife edge, the directions of the tangent and normal vary. Consequently, we need to update the set of cross sections as the knife moves.

Using assumption (A2), we find the endpoints k_1 and k_2 of the arc on the knife edge that will come in contact with the object, as shown in Fig. 4(a). The arc is equally discretized into m linear segments by arc length. Each segment, e_i , has its normal \hat{n}_i and tangent \hat{t}_i . The slice-push ratio for the segment is $\xi_i = \tan \beta_i$, where β_i is the angle between \hat{n}_i and the knife velocity v . The segment's movement is tracked by the trajectory of its midpoint (shown as dashed blue lines). Initially, the cross section associated with the segment passes through its midpoint's first point of contact with the object, and is normal to the knife segment (shown as green lines in side view).

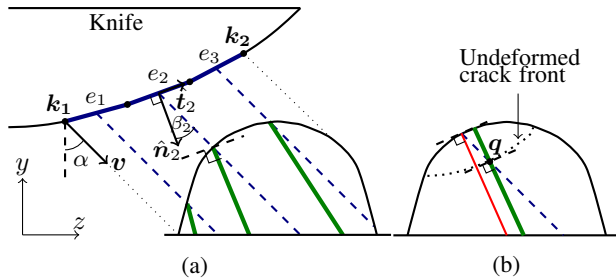


Fig. 4: (a) Discretizing the curved edge into straight segments e_i . Dashed blue lines represent the midpoint's trajectory of each edge segment, solid green lines show the side view of the initial cross sections associated with each segment. (b) Updating old cross section (red). The new cross section (green) passes through the intersection of the crack front (dotted) and midpoint trajectory (dashed, blue).

Unlike the case of a straight knife, as the segment moves, the associated cross section will slide off it, and will not be normal to the new segment of contact. So we need to continuously update the cross section. After some small movement of the knife segment, a new cross section is selected such that it passes through the intersection point q of the crack front and the segment's midpoint trajectory in the undeformed position, and is normal to the knife segment. This new segment is shown as the green line in Fig. 4(b).

The crack front is represented by a second degree polynomial fitted over the crack tip of each cross section.

V. EXPERIMENTS

Three experiments were conducted. The first one was to validate our model for varying fracture toughness during slicing. A straight edge knife was used to slice cuboid pieces around the core of a single object to reduce the influences of geometry and non-homogeneous mechanical properties. The second experiment was to validate our model for cutting with a curved knife edge, again using cuboid pieces.

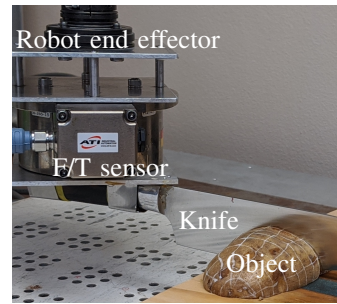


Fig. 5: Experimental setup.

The last experiment was done with objects in their natural shapes to measure modeling accuracy in practical cutting situations. Cutting was carried out by rigidly attaching a kitchen knife to an ADEPT Cobra 800 robot, as shown in Fig. 5. Force and torque data were recorded by a 6-axis F/T sensor (Delta IP65) from ATI Industrial Automation, which was mounted between the knife and the robot's open end. The speed of knife translation was fixed at 0.00625m/s. Each experiment was performed on two objects: a potato and an eggplant. Potatoes are relatively hard and homogeneous, while eggplants are soft and non-homogeneous with fibers running from one end to another. Table I lists the physical parameters for our experiments. Initial values for Young's modulus (E) and Poisson's ratio (ν) were taken from [29] and [30] and then tuned over several cutting trials. The same parameter values were used for the first two experiments where cuboid pieces were cut. These pieces were prepared, as shown in Fig. 6(a), from a single potato (eggplant). A different set of parameter values was used when we cut the whole objects with their skins intact. Also, as an eggplant is soft and has a very tough skin, we set a larger initial fracture toughness and then use a smaller value after fracture due to stress concentration at the crack tip for soft materials.

TABLE I: Mechanical properties of the objects in the experiments: Young's modulus (E), Poisson's ratio (ν), coefficient of blade-material friction (μ), interior fracture toughness (R_c), and initial fracture toughness (R_c').

Object	E (N/m)	ν	μ	R_c (N/m)	R_c' (N/m)
Experiments with cuboid pieces (without skin)					
Potato	2×10^6	0.4	0.1	150	150
Eggplant	0.4×10^6	0.35	1.0	140	275
Experiments with whole objects (with skin)					
Potato	2×10^6	0.4	0.1	230	230
Eggplant	0.55×10^6	0.35	1.0	260	650

A. Slicing With a Straight Knife Edge

Cutting was first carried out using a segment of the knife edge close to the handle. Four cuboid pieces from a potato were used, as shown in Fig. 6(a). Each piece was sliced with a different slice-push ratio, $\xi = \tan \alpha$, where α is the angle between the velocity direction and the y -axis, as

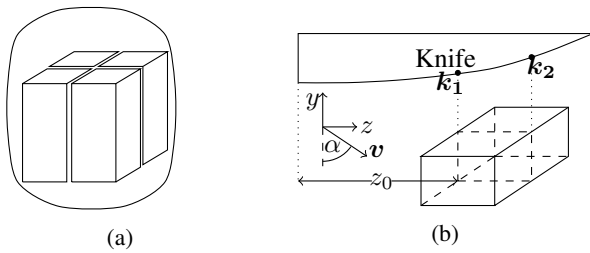


Fig. 6: (a) Piece preparation. (b) Cutting setup: α is the angle between the velocity v and the y -axis, and z_0 is the horizontal distance of the piece from one endpoint of the knife edge.

shown in Fig. 6(b). Fig. 7(a) plots the sensed force per unit length in the vertical y -direction and horizontal z -direction, and the total work per unit length against the vertical knife displacement. Force and work for each piece were divided by its length along the z -axis for comparison. Simulation is done for each piece by slicing one (uniform) 2D cross section using our model, shown in Fig. 7(b). Cutting was repeated for an eggplant. Figs. 7(c) and (d) show the plots for experiment results and simulation, respectively.

The first experiment shows that force and velocity are not coincident during the cutting of deformable objects. For instance, in Fig. 7(a) the horizontal to vertical force ratio does not match the slice-push ratio (ξ) used for the experiment. Also, the fracture toughness does not remain constant. The last column in Fig. 7 shows total work per unit length done by the knife for different ξ values. The total work decreased as ξ increased. But for a very large ξ value, the total work increased for potato. This can be explained by the fact that the decrease in the fracture toughness during slicing saturates at higher ξ values, see Fig. 3, and the work done to overcome friction increases as total displacement increases. Total work for the eggplant shows a considerable decrease for the same case because the object is very anisotropic with fibers running along its axis, and the mechanism for fracture under shear may be very different from compression. This is evident in Fig. 7(c) from the fact that while the horizontal force increases with ξ , it suddenly drops at a very high ξ value. For a potato and for low ξ values for an eggplant, our predictions follow the experiments very closely.

B. Pressing With a Curved Knife Edge

Four new cuboid pieces were prepared as before. Cutting was carried out using different sections of the knife by varying the horizontal distance z_0 of each piece to the left endpoint of the knife edge (where it connects the knife's handle). See Fig. 6(b). The knife moves only vertically downward ($\alpha = 0$). For simulation, the knife edge's cutting section (between k_1 and k_2 in the figure) is discretized into ten segments. A 3D cuboid mesh was created for each piece for generating cross sections, which are updated as described in Section IV for each step of knife displacement by 1 mm. Figs. 8 and 9 show the experiment results and our simulation for potato and eggplant, respectively.

As illustrated in Fig. 6(b), the knife edge curves more as z_0 increases, resulting in a longer duration to establish contact with the object. For a potato, fracture happened very early

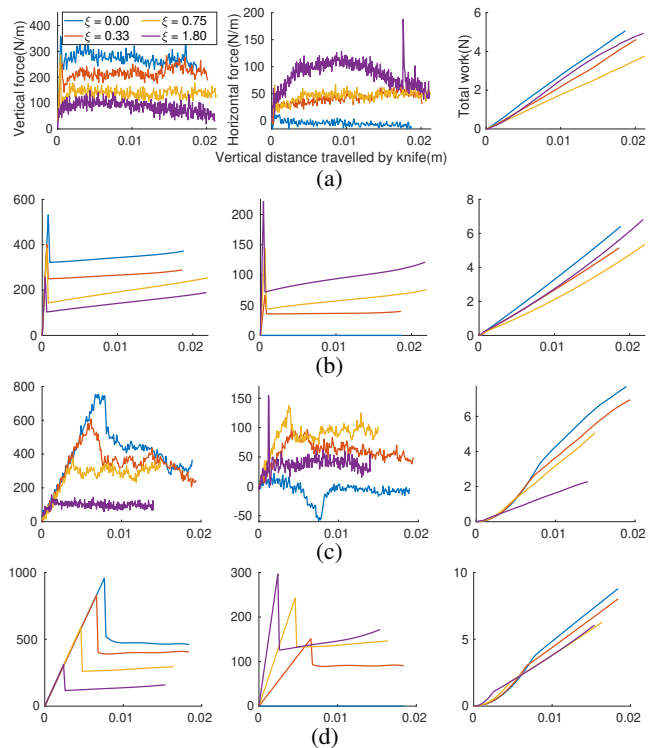


Fig. 7: Experiment results and simulation for straight knife edge slicing of cuboid objects with slice-push ratio $\xi = \{0, 0.33, 0.75, 1.8\}$. The vertical force (y -direction), the horizontal force (z -direction) and the total work, plotted in the three columns, respectively, are divided by the length of the cuboid along the z -direction (see Fig. 6(b)). (a) Experiment on a potato cuboid. (b) Simulation for the experiment (with column correspondence). (c) Experiment on an eggplant. (d) Its simulation. In every plot the horizontal axis is knife displacement in the downward y -direction.

on. Fig. 8 shows that the slopes of force and work decreased in the meantime, before they were stabilized at the maximum contact by the knife edge. Fig. 9 shows that fracture of an eggplant happened very late, with the effect of increasing z_0 value reflected in the initial slopes of the vertical force plots. Since the horizontal force was negligible, its sensed value was not accurate, especially in the case of cutting a potato. Our predictions for both potato and eggplant are very close to the experiment results.

C. Slicing Natural Shapes With a Curved Knife Edge

Three half-potatoes were prepared beforehand with a flat base to stabilize them on the cutting board (see Fig. 5). The experiments were conducted by varying z_0 and α for each piece. For simulation, every piece was laser scanned to generate a 3D mesh. Figs. 10 and 11 show the experiment results and simulation for potato and eggplant, respectively.

Our model predicts the forces and work reasonably well considering three different potatoes (eggplants) were cut. Tough skin on the eggplant decreases the horizontal force prediction accuracy as our generalized plane strain assumption may no longer be valid.

VI. DISCUSSION

We have proposed a model for characterizing the change in fracture toughness during slicing based on critical maximum

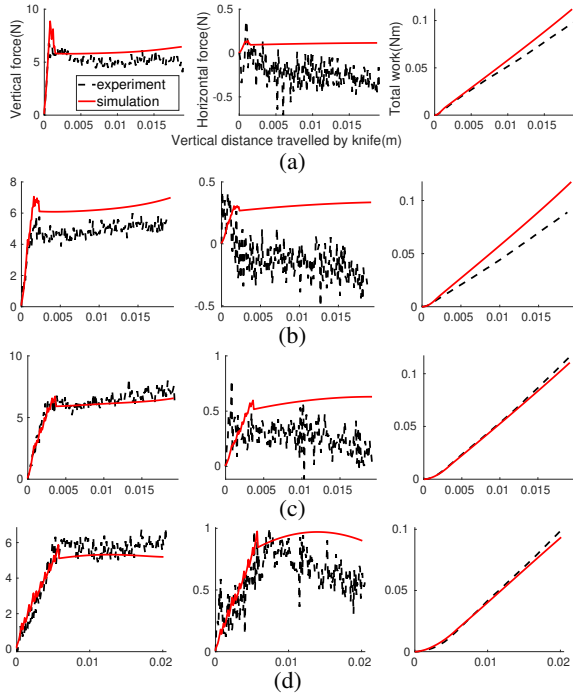


Fig. 8: Vertical and horizontal forces, and total works from cutting four cuboid potato pieces generated by a curved knife edge translating vertically downward (cf. Fig. 6(b)). Cutting was performed using different sections of the knife edge with z_0 values: (a) 0.02 m, (b) 0.0765 m, (c) 0.1135 m, and (d) 0.14 m. The horizontal axis is knife displacement in the downward y -direction. In each diagram, black dots represent the experimental result and the red curve represents the simulation result.

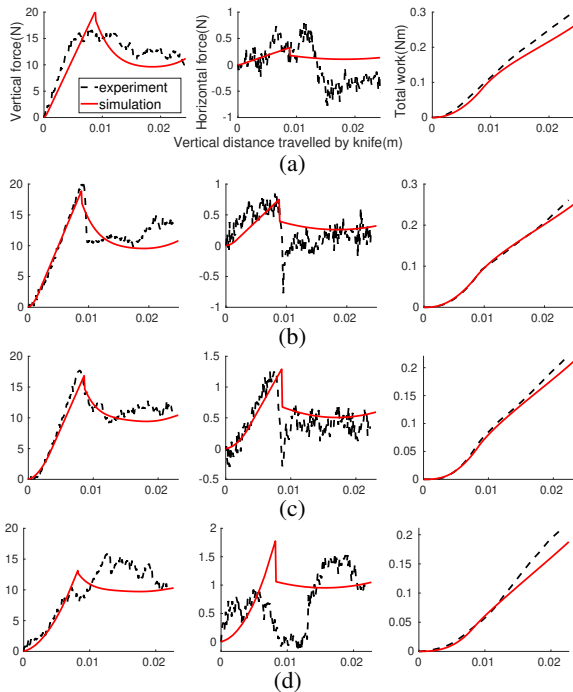


Fig. 9: Experiment results and simulation for cutting cuboid eggplant pieces by a curved knife edge moving vertically downward. Same sequence of four values of z_0 as given in Fig. 8 were used.

principal strain. This model can be combined with our previous work to correctly predict the forces during cutting

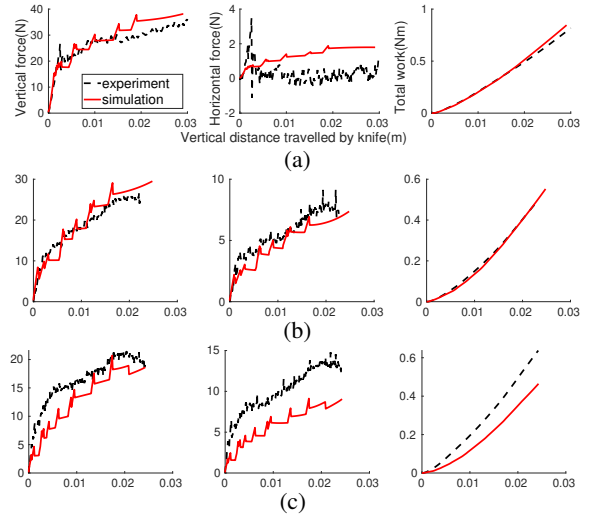


Fig. 10: Experiment results and simulation for cutting general shaped potatoes by a curved knife edge, where (α, z_0) takes on the values: (a) $(0^\circ, 0.046\text{m})$ (b) $(24^\circ, 0.087\text{m})$, and (c) $(45^\circ, 0.139\text{m})$. The horizontal axis is knife displacement in the downward y -direction.

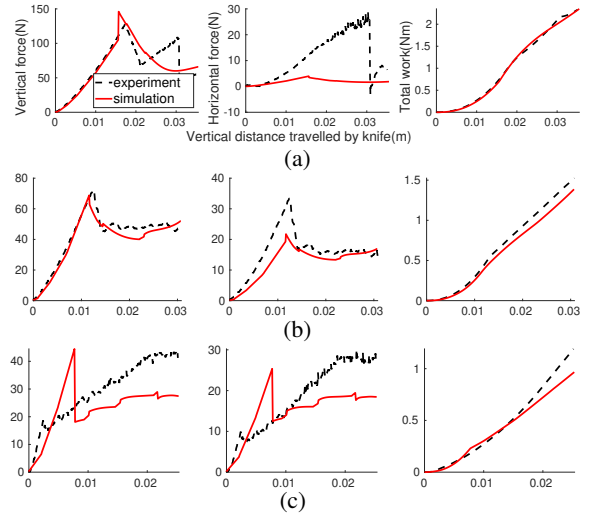


Fig. 11: Experiment results and simulation for cutting general shaped eggplants by a curved knife edge. Same three pairs of values of (α, z_0) as in Fig. 10 were used sequentially.

by slicing. In addition, we have also proposed a method to model the effect of knife geometry by dynamically updating cross sections according to the knife trajectory and crack front position during cutting. As seen from the experiments, our model predicted cutting forces during slicing with curved knife edge with reasonable accuracy for potato and eggplant.

Our current model is limited by the varying mechanical properties of the foods. In the future, we would like to predict them based on the history of the cut. Effects of tough skin on the fruits and vegetables as well as anisotropic structures like fibers also need to be explored in depth. Further investigation on the role played by friction during slicing is needed. We would also like to explore application of our model in knife control to achieve smooth cutting of non-homogeneous objects.

REFERENCES

- [1] P. Jamdagni, and Y.-B. Jia. "Robotic cutting of solids based on fracture mechanics and FEM," in *Proc. IEEE/RSJ Int. Conf. Intell. Robots Syst.*, 2019, pp. 8246–8251.
- [2] A. G. Atkins, X. Xu, and G. Jeronimidis. "Cutting, by 'pressing and slicing,' of thin floppy slices of materials illustrated by experiments on cheddar cheese and salami," *J. Materials Sci.*, vol. 39, pp. 2761–2766, 2004.
- [3] T. L. Anderson. *Fracture Mechanics: Fundamentals and Applications*. CRC Press, Boca Raton, FL 33487-2742, US, 2005.
- [4] A. H.-D. Cheng, J. J. Rencis, and Y. Abousleiman. "Generalized plane strain elasticity problems," *Trans. Model. Simul.*, vol. 10, pp. 167–174, 1995.
- [5] E. Reyssat, T. Tallinen, M. Le Merrer, and L. Mahadevan. "Slicing softly with shear," in *Phys. Rev. Lett.*, vol. 109, pp. 244301-1–244301-5, 2012.
- [6] A. G. Atkins. "Toughness and cutting: a new way of simultaneously determining ductile fracture toughness and strength," *Engr. Fracture Mechanics*, vol. 72, pp. 850–860, 2004.
- [7] M. Khadem, C. Rossa, R. S. Sloboda, N. Usmani, and M. Tavakoli. "Mechanics of tissue cutting during needle insertion in biological tissue," *IEEE Robot. Autom. Letters*, vol. 1, no. 2, pp. 800–807, 2016.
- [8] C. Gokgol, C. Basdogan, and D. Canadinc. "Estimation of fracture toughness of liver tissue: Experiments and validation," *Medical Engr. Phys.*, vol. 34, pp. 882–891, 2012.
- [9] T. Azar and V. Hayward. "Estimation of the fracture toughness of soft tissue from needle insertion," in *LNCS*, Springer-Verlag Berlin, 2008, pp. 166–175.
- [10] T. Chanthasopeephan, J. P. Desai, and A. C. W. Lau. "Modeling soft tissue deformation prior to cutting for surgical simulation: Finite analysis and study of cutting parameters," *IEEE Trans. Biomed. Engr.*, vol. 54, no. 3, pp. 349–359, 2007.
- [11] B. Ghali and S. Sirouspour. "Nonlinear finite element-based modeling of soft tissue cutting," in *Proc. IEEE Toronto Int. Conf. Sci. Tech. Humanity*, 2009, pp. 141–146.
- [12] B. Takabi, and B. L. Tai. "A review of cutting mechanics and modeling techniques for biological materials," *Medical Engr. Phys.*, 45:1–14, 2017.
- [13] D. Zhou and G. McMurray. "Modeling of blade sharpness and compression cut of biomaterials," *Robotica*, vol. 28, pp. 311–319, 2010.
- [14] D. Zhou, M. R. Claffee, K.-M. Lee, and G. V. McMurray. "Cutting, 'by pressing and slicing', applied to robotic cutting bio-materials, Part I: Modeling of stress distribution," in *Proc. IEEE/RSJ Int. Conf. Intell. Robots Syst.*, 2006, pp. 2896–2901.
- [15] D. Zhou, M. R. Claffee, K.-M. Lee, and G. V. McMurray. "Cutting, 'by pressing and slicing', applied to robotic cutting bio-materials, Part II: Force during slicing and pressing cuts," in *Proc. IEEE/RSJ Int. Conf. Intell. Robots Syst.*, 2006, pp. 2256–2261.
- [16] A. G. Atkins and X. Xu. "Slicing of soft flexible solids with industrial applications," *Int. J. Mech. Sci.*, vol. 47, pp. 479–492, 2005.
- [17] K.-R. Deibel, C. Raemy, and K. Wegener. "Modeling slice-push cutting forces of a sheet stack based on fracture mechanics," *Engr. Fracture Mechanics*, vol. 124–125, pp. 234–247, 2014.
- [18] K.-R. Deibel, S. Lämmlein, and K. Wegener. "Model of slice-push cutting forces of stacked thin material," *J. Materials Processing Technology*, vol. 214, pp. 667–672, 2014.
- [19] A. Spagnoli, R. Brighenti, M. Terzano, and F. Artoni. "Cutting resistance of soft materials: Effects of blade inclination and friction," *Theo. Appl. Fracture Mechanics*, vol. 101, pp. 200–206, 2019.
- [20] J. Wang, C. Li, and S.-C. Chen. "Sectioning soft materials with an oscillating blade," *Precision Engineering*, vol. 56, pp. 96–100, 2019.
- [21] G. Zeng and A. Hemami. "An adaptive control strategy for robotic cutting," in *Proc. IEEE Int. Conf. Robot. Autom.*, 1997, pp. 22–27.
- [22] S. Jung and T. C. Hsia. "Adaptive force tracking impedance control of robot for cutting nonhomogeneous workpiece," in *Proc. IEEE Int. Conf. Robot. Autom.*, 1999, pp. 1800–1805.
- [23] P. Long, W. Khalil, and P. Martinet. "Modeling and control of a meat-cutting robotic cell," in *Proc. Int. Conf. Advanced Robot.*, 2013, pp. 61–66.
- [24] P. Long, W. Khalil, and P. Martinet. "Force/vision control for robotic cutting of soft materials," in *Proc. IEEE/RSJ Int. Conf. Intell. Robots Syst.*, 2014, pp. 4716–4721.
- [25] X. Mu, Y. Xue, and Y.-B. Jia. "Robotic cutting: Mechanics and control of knife motion," in *Proc. IEEE Int. Conf. Robot. Autom.*, 2019, in press.
- [26] N. Perez. *Fracture mechanics*. Kluwer Academic Publishers, 2004.
- [27] J. Boussinesq. *Application des Potentiels a l'Etude de l'Equilibre et du Mouvement des Solides Elastiques*. Gauthier-Villars, Paris, 1885.
- [28] R. O. Davis, A. P. S. Selvadurai. *Elasticity and Geomechanics*. Cambridge University Press, New York, US, 1996.
- [29] M. Bentini, C. Caprara, R. Martelli. "Physico-mechanical properties of potato tubers during cold storage," in *Biosystems Engineering*, vol. 104, pp. 25–32, 2009.
- [30] S. M. Ashtiani, M. R. Golzarian, J. B. Motie, B. Emadi, N. N. Jamal, H. Mohammadinezhad. "Effect of loading position and storage duration on the textural properties of eggplant," in *Int. J. Food Properties*, vol. 19, pp. 814–825, 2016.